Advanced Powder Technology 32 (2021) 2517–2529

Contents lists available at ScienceDirect

Advanced Powder Technology

journal homepage: www.elsevier.com/locate/apt

Original Research Paper

Kernel identification in continuous fluidized bed spray agglomeration from steady state data

Eric Otto [a,*], Robert Dürr [b], Gerd Strenzke [c], Stefan Palis [a,e], Andreas Bück [d], Evangelos Tsotsas [c], Achim Kienle [a,b]

[a] Automation/Modelling, Otto-von-Guericke-University Magdeburg, Universitätsplatz 2, 39106 Magdeburg, Germany
[b] Process Synthesis and Process Dynamics, Max Planck Institute for Dynamics of Complex Technical System, Sandtorstrasse 1, 39106 Magdeburg, Germany
[c] Thermal Process Engineering, Otto-von-Guericke-University Magdeburg, Universitätsplatz 2, 39106 Magdeburg, Germany
[d] Institute of Particle Technology, Friedrich-Alexander-Universität Erlangen-Nürnberg, Cauerstraße 4, 91058 Erlangen, Germany
[e] National Research University "Moscow Power Engineering Institute", Moscow, Russia

ARTICLE INFO

Article history:
Received 30 September 2020
Received in revised form 16 April 2021
Accepted 14 May 2021
Available online 7 June 2021

Keywords:
Continuous spray agglomeration
Parameter identification
Population balance equation
Agglomeration kernel
Kapur kernel

ABSTRACT

Fluidized bed spray agglomeration is an important industrial particle formation process. In particular, the continuous operation mode is able to provide a constant stream of product particles with constant quality in terms of particle properties. Mathematical process modeling represents a valuable tool for a thorough analysis of the involved mechanistic processes and can further be used for process intensification and control. Sophisticated models describing the quantitative effect of process conditions on particle properties are particularly important. Therefore, in this contribution the influence of the seven most important operational parameters on the particle size distribution is modeled, including fluidization and binder properties. To this end, a population balance process model with the three-parametric Kapur kernel is fitted to experimental data. The first main result of this contribution is the quantitative description of the dependency between the agglomeration rate and the process conditions by multidimensional paraboloids. The second main result is the introduction of a general method by which this quantitative formulation is obtained.

1. Introduction

Since a large proportion of substances used in the chemical engineering industry is particulate matter, there is great interest in the investigation and understanding of the according production processes. Fluidized bed spray agglomeration (FBSA) is such a particle formation process, which is widely used industrially, due to the possibility of producing agglomerates with tailor-made properties, such as particle size and particle porosity [4]. Examples of applications are the refinement of milk powder in the food industry, production of fertilizers in the agricultural industry and powdery drugs in the pharmaceutical industry [2,31,30].

In these processes a binder is sprayed into a fluidized particle bed. Agglomerates are created from primary particles when the binder solution between two particles in contact dries and solid bridges are formed. The formed agglomerates can grow further by coalescence with additional particles as presented in Fig. 1. One advantage of continuous FBSA is the high production rate due to large contact surfaces and good heat and mass transfer in the fluidized bed. Another one is the possibility to adjust desired particle properties such as size, porosity, flowability and hardness by variation of several process conditions. While the latter is accomplished by using simple heuristics in most industrial applications, more structured approaches are an active field of research [6,7,41] with the ultimate goal of providing the possibility of producing particles with specifically defined properties.

The goal of this contribution is to establish a method by which the experimentally identified influence of process conditions on particle properties can be incorporated in a mathematical process model. Furthermore this method is applicable to a wide range of particle processes such as polymerization, crystallization and cell aggregation processes. In this contribution the experimental findings in Strenzke et al. [38] are used to derive the process model for FBSA.

A process model that incorporates the effects of process parameters on the process kinetics and product agglomerate properties can be used for process design, optimization and model based con-

* Corresponding author.
E-mail address: eric.otto@ovgu.de (E. Otto).

https://doi.org/10.1016/j.apt.2021.05.028

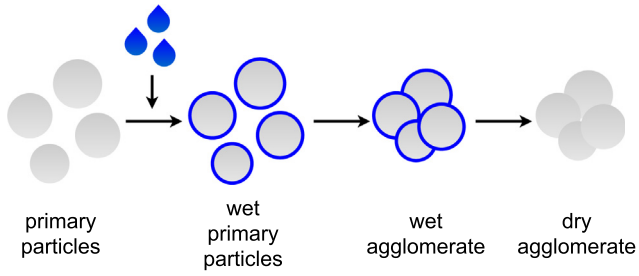

Fig. 1. Process scheme including the three steps of agglomeration: Wetting, collision and dyring.

trol [3,29]. Modeling the influence of process parameters in fluidized bed processes has been investigated in numerous contributions mainly focusing on batch operation. In Murtoniemi et al. [26] the influence of several process conditions on particle size and friability was modeled by artificial neural networks for fluidized bed granulation, however only mean granule sizes were considered. Tan et al. [39] used a physically based approach for fluidized bed melt granulation in order to model the effect of process parameters on the particle size distribution. In Terrazas-Velarde et al. [40] Monte-Carlo-Simulations (MCS) were utilized for FBSA, using knowledge of the underlying micro-processes. The Monte-Carlo methods however, are inappropriate for model based control due to the high computational effort. Furthermore, the underlying micro-processes are very complex and not yet completely investigated. Hussain et al. [17,18] used the MCS approach to parametrize a differential equation and predict particle size distributions. Since these approaches often rely on a profound understanding of the underlying mechanisms, are computationally expensive or are restricted to a very specific field of application, empirical models present a commonly used alternative to describe the process dynamics [14,32,1]. An established framework for modeling the dynamics of agglomeration processes by partial differential equations is the population balance equation (PBE) [33]

$$\frac{\partial n}{\partial t} = \frac{1}{2}\int_0^v \beta(t,u,v-u)n(t,u)n(t,v-u)du - \int_0^\infty \beta(t,v,u)n(t,v)n(t,u)du. \quad (1)$$

Here the so-called agglomeration kernel $\beta(t,u,v)$ contains information on the mechanisms of the agglomeration, e.g. dependence on the particle volumes u and v and process parameters like bed temperature. As previously pointed out, the direct mechanisms are not known and thus empirical kernels are commonly used. In the literature a variety of parame-trized kernel functions is proposed.

In this contribution a new approach in kernel estimation based on least-squares-function fitting [14] and utilizing the population balance model of the continuous FBSA process is presented. It will be shown that the kernel parameters are structurally identifiable and, furthermore, a functional dependence between process and kernel parameters is unveiled, which is crucial in order to use the model for the intended purposes.

The remainder of this article is structured as follows: In Section 2 the process itself and the process model are described briefly. The subsequent chapter is concerned with presenting the parameter estimation algorithm including the computation of parameter confidence intervals as well as an investigation of structural identifiability. In Section 4 the experimental data and the identification results are presented and the influence of the process parameters is described as arguments in the kernel function. Furthermore the validity of the obtained parameters is discussed. The contribution closes with conclusions and an outlook on further research.

2. Process description and process model

In this section the process including the relevant process parameters as well as the mathematical process model are presented briefly. A more detailed description including a discussion of the influence of several process parameters on the product properties can be found in [38].

In the continuous operation mode, schematically presen-ted in Fig. 2, primary particles with a specified volume are continuously fed into the process chamber. The particle feed rate $\dot{M}_{\text{feed}}$ can be adjusted. The bed is fluidized by a pre-heated air flow with temperature $T_{\text{g,in}}$ and mass flow rate $\dot{M}_{\text{FA}}$. The binder solution is sprayed onto the particle bed through a nozzle with mass flow rate $\dot{M}_{\text{spray}}$. The size of the dispersed droplets can be adjusted by varying the air volume flow rate through the nozzle $\dot{V}_{\text{NA}}$. The binder mass content in the injected solution is denoted with x_{b}. The particle removal is handled by a classifying airflow whose velocity is adjusted such that particles exceeding a certain mass fall through a classifying tube. The respective volume flow rate is denoted by $\dot{V}_{\text{CA}}$.

In the following, a suitable mathematical process description is presented. In order to characterize a collective of particles with distributed properties, the number density function (NDF) $n(t,\mathbf{x})$ is introduced, where $\mathbf{x}$ is a set of internal or external coordinates. Internal coordinates are usually particle properties, external coordinates specify the position in space. Since the fluidized particle bed is assumed to be ideally mixed, the spatial (external) coordinates are neglected. Furthermore, the agglomerate volume has been shown to be a key property [4], having a significant impact on other particle properties. Therefore, in this contribution this property is considered, i.e. $\mathbf{x} = v$, where v is the characteristic

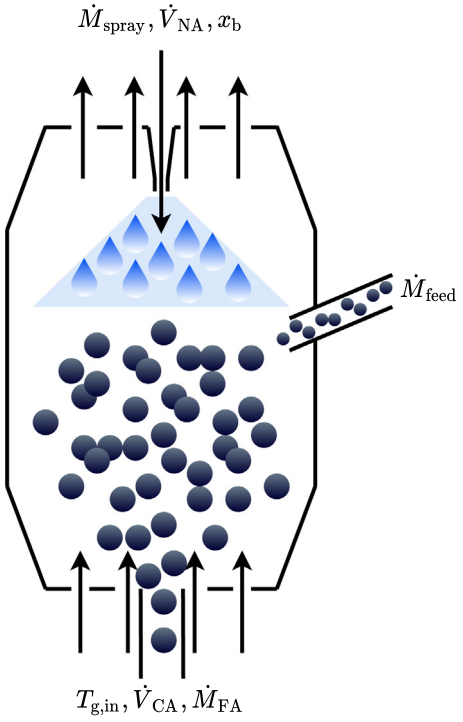

Fig. 2. Schematic illustration of the process with particle feed and spraying into the process chamber, fluidization and separating outlet.

particle volume v. A volume-equivalent representative diameter d can be computed by using

$$v = \frac{\pi}{6} d^3. \tag{2}$$

The NDF $n(t, v)$ describes the number density of particles with volume interval v at time t in the fluidized bed. Alternatively the particle collective can be characterized by its normalized volume distribution (NVD) $q_3(t, d)$ which is computed by

$$q_3(t, d) = \frac{d^3 n(t, d)}{\int_0^\infty d^3 n(t, d) \mathrm{d}d} \tag{3}$$

with

$$n(t, d) = n(t, v) \frac{\mathrm{d}v}{\mathrm{d}d}. \tag{4}$$

A standard approach for modeling the evolution of the NDF is using the population balance equation (PBE) [33]

$$\frac{\partial n(t, v)}{\partial t} = \dot{n}_{\text{feed}}(t, v) + \dot{n}_{\text{agg}}(t, v) - \dot{n}_{\text{out}}(t, v) \tag{5}$$

where the three terms on the right-hand-side describe fluxes by particle feed $\dot{n}_{\text{feed}}$ and removal $\dot{n}_{\text{out}}$ as well as particle aggregation $\dot{n}_{\text{agg}}$. The change in particle volume due to binder addition is neglected in the PBE due to its low volume contribution. In the following, the three terms will be examined more closely.

The feed term

$$\dot{n}_{\text{feed}}(t, v) = \dot{N}_{\text{feed}}(t) q_{0,\text{feed}}(v) \tag{6}$$

consists of the normalized number density distribution of the fed particles

$$q_{0,\text{feed}}(v) = \frac{n_{\text{feed}}(v)}{\int_0^\infty n_{\text{feed}}(v) \mathrm{d}v} \tag{7}$$

and their number feed rate $\dot{N}_{\text{feed}}$. Since the former is known, the latter can be computed from the mass feed rate $\dot{M}_{\text{f}}(t)$ which is constant during the process.

The particle outlet is modeled by

$$\dot{n}_{\text{out}}(t, v) = K(t) T(t, v) n(t, v), \tag{8}$$

where $K(t)$ is the removal rate and $T(t, v)$ the separation function, which accounts for the classifying character of the outlet. The term $T(v)n(t, v)$ furthermore reflects the particle size distribution of the product particles at time t. There are different approaches to the modeling of K and T based on properties of the particle bed and the classification air flow [15,27]. However, in this contribution we choose to compute both functions based on the actual measured product mass flow and the product particles' size distribution. This is motivated by the idea of minimizing the modeling error of the outlet so that it does not affect the identification of the kernel parameters.

Hence, $T(t, v)$ and $K(t)$ are computed in two steps using the measurements of the bed and product NVDs $q_{3,b}(t, d)$ and $q_{3,\text{p}}(t, d)$ and the product mass flow rate $\dot{m}_{\text{p}}(t)$. At first, the separation function is computed such that the measured product distribution results from the measured bed distribution at every measurement time instant. Then $K(t)$ is computed such that the measured product mass withdrawal $\dot{m}_{\text{p}}(t)$ results from the measured bed mass and volume distribution given the computed separation function. During the process simulation, $K(t)$ and $T(t, v)$ are interpolated linearly between the measurement times.

In order to compute the separation function with respect to particle diameter d, it is approximated by N weighted ansatz-functions $\varphi_n(d)$

$$T(d, a_n) = \sum_{n=1}^{N} a_n \varphi_n(d). \tag{9}$$

The chosen ansatz functions are cumulative Gaussian functions with the different mean values and same standard deviation scattered on the expected diameter interval. In order to find the weights a_n, the following optimization problem is solved at every measurement time instant:

$$min_{a_n} || q_{3,\text{p}}(d) - \frac{T(d, a_n) d^3 n_{\text{b}}(d)}{\int_0^\infty T(d, a_n) d^3 n_{\text{b}}(d) \mathrm{d}d} ||_2^2, \tag{10}$$

where $n_{\text{b}}(d)$ is computed from $q_{3,b}(d)$. The separation function $T(d)$ is transformed into $T(v)$ using Eq. 2. In the second step K is computed such that the measured bed mass withdrawal rate $\dot{m}_{\text{p}}$ results from the measured NDF and the computed separation function, i.e. it solves

$$\dot{m}_{\text{p}} = \varrho_{\text{agg}} \int_0^\infty v (K T(v) n_{\text{b}}(t, v)) \mathrm{d}v, \tag{11}$$

where the integral term represents the total volume flow of product particles. Since the particles are porous, the apparent agglomerate density differs from the primary particle density. In this contribution an average agglomerate density is computed from the total mass and volume of bed samples [38].

An alternative to the optimization approach presented here is the use of online-parameter estimation algorithms for $K(t)$ and $T(v)$ which have been shown to be effective for similar particle processes [28,13,9].

The particle coalescence is modeled with the agglomeration term $\dot{n}_{\text{agg}}(t, v)$. It is based on a binary aggregation where two particles with volume u and $v - u$ form a new particle with volume v [16]. The agglomeration term accounts for the "birth and "death" of particles with volume v:

$$\begin{aligned} \dot{n}_{\text{agg}}(t, v) &= B(t, v) - D(t, v) \\ &= \tfrac{1}{2} \int_0^v \beta(t, u, v-u) n(t, u) n(t, v-u) \mathrm{d}u \\ &\quad - \int_0^\infty \beta(t, v, u) n(t, v) n(t, u) \mathrm{d}u, \end{aligned} \tag{12}$$

where $\beta(t, u, v)$ is the agglomeration kernel describing the probability and frequency of a coalescence event as a function of the particle size. The kernel is separated into a time- and a volume-dependent part

$$\beta(t, u, v) = \beta_0(t) \beta(u, v) \tag{13}$$

as commonly assumed, whereby β_0 denotes the agglomeration efficiency and $\beta(u, v)$ is called coalescence kernel [35].

As a key term for understanding the process of agglomeration, the coalescence kernel can take various forms depending on the actual process setting. In the literature kernels are proposed for particles being subject only to Brownian movement [37] or gravitational forces [42], or particles behaving according to kinetic theory [36]. Generally, these kernel functions are limited to special processes and not applicable to the FBSA process considered here, where the interconnection of physical mechanisms is rather complicated (collision dynamics, coalescence depending on material properties of binder solution and particulate matter). Hussain et al. [17,18] constructed a kernel specifically for FBSA in batch operation based on a physically motivated MCS. However, as mentioned earlier the underlying micro-processes are not yet fully investigated, therefore an alternative to this approach is the use of purely empirical kernels customized for the respective process. In the literature a variety of kernels, sometimes with adjustable parameters, is proposed. In Table 1 a selection of commonly used

Table 1
Selection of empirical coalescence kernels from the literature.

Kernel	Formula	Source
Constant	$\beta(u,v)=1$	Kapur and Fuerstenau [21]
Sum	$\beta(u,v)=u+v$	Golovin [12]
Product	$\beta(u,v)=uv$	Golovin [12]
Kapur	$\beta(u,v)=\frac{(u+v)^a}{(uv)^b}$	Kapur [20]
Polynomial	$\beta(u,v)=a_0+a_1u+a_2v+a_3u^{-1}+a_4v^{-1}\dots$	Eisenschmidt et al. [10]

empirical coalescence kernels is presented. Due to the considerations above this contribution focuses on empirical agglomeration kernels.

3. Parameter identification

In this section the parameter identification algorithm, including the computation of confidence intervals and checking structural identifiability, is described.

In order to identify a vector $\mathbf{p}=(p_1,\dots,p_N)$ of N free model parameters from steady state data, such as the agglomeration rate β_0 and coalescence kernel parameters, from experimental data, the following minimization problem has to be solved:

$$\min_{\mathbf{p}} \quad J(\mathbf{p}) \tag{14}$$

with the objective function

$$J(\mathbf{p})=\|u_{\text{meas}}(d)-u_{\text{sim}}(d,\mathbf{p})\|_2 \tag{15}$$

where $u(d)$ is defined as [14]

$$u(d)=d^3n(d) \tag{16}$$

and $n(d)$ is the steady state size distribution in the fluidized bed as a function of the particle diameter d. For the measurements u_{meas} is computed from CamSizer measurements of the steady state NVD $q_{3,\text{meas}}(d)$, bed mass m_{meas} and mean agglomerate density ϱ under the assumption of spherical particles. The simulated counterpart u_{sim} is computed by using Eqs. 16 and 2 for the steady state solution of the PBE model. The latter is obtained by solving the partial differential equation numerically for a sufficiently long time, such that a stable steady state is reached. In order to do this, the PBE is spatially discretized using the cell-average technique introduced by Kumar et al. [23]. The resulting ODE system is solved using the integrated solver `ode15s` in *MATLAB R2018b*. The solution of the minimization problem (Eq. 14) is obtained by using an interior-point algorithm with quasi-Newtonian approximation of the Hessian matrix which is implemented in *MATLAB* using `fmincon`. An alternative method for parameter identification used for particle processes which is additionally capable of identifying parameters online is described in Golovin et al. [13].

In order to validate the meaningfulness of the identified parameters two additional properties are checked: Structural identifiability of the parameters gives information about the uniqueness of the estimated parameters [34,8], confidence intervals are intervals around the parameter estimates to which the actual parameters can be be narrowed with a certain probability.

Structural identifiability of a parameter p_i is checked using profile likelihoods. For an identified vector of optimal parameters $\mathbf{p}^{\text{opt}}=(p_1^{\text{opt}}\,p_2^{\text{opt}}\dots p_N^{\text{opt}})$ the parameter p_i is locally structurally identifiable if its profile likelihood

$$J_{\text{PL}}(p_i)=\min_{p_j\neq p_i} \quad J(\mathbf{p}) \tag{17}$$

has a unique minimum in the neighborhood of $\mathbf{p}^{\text{opt}}$. The minimization results in a one-dimensional curve for every parameter p_i. The model is said to be structurally identifiable if every curve J_{PL} has a distinct minimum. Non-identifiability of a parameter means that there exist multiple sets of parameters that minimize the objective function.

Confidence intervals give information about the sensitivity of the parameter estimation to measurement noise and are thereby a measure of uncertainty of the determined estimates. Usually, a large number of experiments is required in order to compute these intervals. However, due to the high experimental effort and cost of the agglomeration process only a limited number of experiments can be conducted. In order to overcome this obstacle, bootstrap methods with sets of artificial measurement can be exploited [19].

In a first step a large set of replicated measurements $\mathbb{Y}=(y_1\,y_2\,\dots\,y_M)$ is created. Therefore an absolute, volume-independent normal distribution of measurement errors $\mathcal{N}(\mu,\sigma)$ is assumed and parametrized with the actual measurement data. Then for every element of $\mathbb{Y}$ a new optimal parameter vector $\mathbf{p}^{\text{opt}}$ is identified. The confidence intervals for parameters p_i are calculated using the percentile method. If p^{α} is the $100\cdot(1-\alpha)$-percentile of M bootstrap replications, then the confidence interval is computed by

$$\left[p_i^{\text{lo}},p_i^{\text{up}}\right]=\left[p_i^{\alpha/2},p_i^{1-\alpha/2}\right]. \tag{18}$$

Tight confidence interval bounds indicate low sensitivity of the parameter identification with respect to measurement noise and thereby reliable parameter estimates.

4. Results

In the following section the parameter estimation results are presented and interpreted. At first a brief overview of the experiments conducted and published in Strenzke et al. [38] is given and presented in Table 2. In total 15 experiments were conducted and seven parameters were varied. Every experiment took two hours in which 28 samples of the particle bed and 14 samples of the product were drawn. The particle size distribution of the last sample represents the steady state and was used to conduct the parameter estimation. The particle size distribution in these samples was measured with a CamSizer, based on image analysis.

4.1. Reference experiment

In the first subsection optimal parameters are identified for the reference experiment. Then the structural identifiability is checked and confidence intervals are computed.

4.1.1. Parameter identification

In the following the PBE is fitted to the reference experiment measurements using different kernel functions. At first the coalescence kernel $\beta(u,v)=1$ is used, as the volume-independent kernel has no parameters and is the simplest, empirical kernel function. Since the time-independent agglomeration efficiency β_0 is the only parameter to be fitted, a globally optimal value is easy to obtain. In Fig. 3 the normalized volume distributions $q_3(x)$ at steady state, simulated with the optimal parameter $\beta_0^{\text{opt}}=0.248\cdot10^{-10}$ is presented. Furthermore, it is compared to the measured PSD. Clearly, the function fit is not satisfying. Since the volume-independent kernel is not able to describe the agglomeration outcome appropriately further investigations are not conducted.

Instead a more sophisticated coalescence kernel is used. The Kapur kernel

$$\beta(u,v)=\beta_0\frac{(u+v)^a}{(uv)^b} \tag{19}$$

Table 2
Overview of experiments and varied parameters.

	Parameter						
	$\dot{M}_{feed}$ g/min	$\dot{M}_b$ g/min	$T_{g,in}$ °C	x_b %	$\dot{V}_{NA}$ l/min	$\dot{M}_{FA}$ kg/h	$\dot{V}_{CA}$ l/min
REF	250	45	90	4	60	275	415
F1	**150**	45	90	4	60	275	415
F2	**350**	45	90	4	60	275	415
S1	250	**40**	90	4	60	275	415
S2	250	**50**	90	4	60	275	415
T1	250	45	**80**	4	60	275	415
T2	250	45	**100**	4	60	275	415
NA1	250	45	90	4	**40**	275	415
NA2	250	45	90	4	**120**	275	415
FA1	250	45	90	4	60	**260**	415
FA2	250	45	90	4	60	**290**	415
CA1	250	45	90	4	60	275	**400**
CA2	250	45	90	4	60	275	**430**
BC1	250	45	90	**2**	60	275	415
BC2	250	45	90	**6**	60	275	415

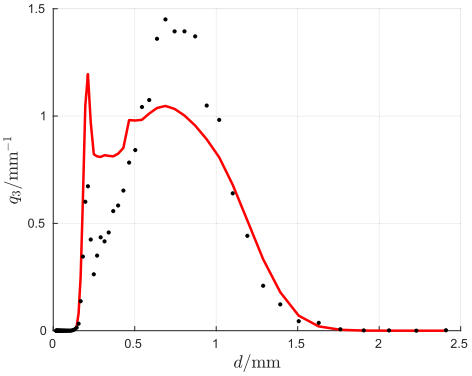

Fig. 3. Measured (black) and simulated (red) NVD at steady state for the reference experiment with volume-independent kernel.

is a two-parametric kernel first proposed in Kapur [20]. For $a = 1$ and $b = 0$ it reduces to the sum kernel, for $a = 0$ and $b = -1$ it reduces to the product kernel. Previous research [32] has shown that a PBM with this kernel is able to provide good fitting results for FBSA, moreover with only three parameters to fit the computational effort is significantly smaller compared to a polynomial approach. In the following the parameter vector $\mathbf{p} = [a, b, \beta_0]$ is estimated.

Solving the minimization problem (Eq: 14) for various initial values shows that two problems can occur.

1. The optimization reaches a local minimum that is clearly not a global minimum. An example for such an optimization result is presented in the first row of Table 3. In the present case, an explanation for this is that measurement noise induces local minima at random points in the parameter space to which the local solver converges. In order to overcome this problem, ℓ_1-trend filtering [22] is applied to the measured data for this and every following optimization. This filter is chosen because in contrast to many other filtering techniques, the primary particle peak in the particle size distribution is not reduced significantly.
2. Different combinations of the three parameters minimize the objective function equally good. Examples of two such combinations are presented in rows two and three in Table 3.

The latter suggests that there exist multiple local minima in the parameter space which indicates non-identifiability of the model due to over-parametrization. In order to find an optimal solution for Eq. 14 with the minimal number of necessary parameters, the objective function is regularized according to the least absolute shrinkage and selection operator (LASSO) method [5]:

$$J^*(\mathbf{p}) = J(\mathbf{p}) + \gamma \|\mathbf{p}\|_1, \tag{20}$$

with $\gamma = 0.01$. Using the ℓ_1-regularization represented by the second term in Eq. 20, an optimal solution with minimal cardinality can be found, i.e. parameters that can be zero become zero. Solving the regularized optimization problem gives the optimal parameters presented in the fourth row of Table 3, where $a = 0$ and the objective function value is still minimal. This suggests that $(u + v)^a = 1$ holds for this FBSA process.

In order to further investigate this, J is sampled at selected points in the parameter space $(a, b, \beta_0) \in \mathbb{R}^3$. Therefore the intervals $a, b \in (-1, 1)$ are discretized into $N = 81$ and the interval $\log_{10}(\beta_0) \in (-45, -5)$ into $N = 401$ equidistant points. The resulting function of three arguments is reduced, by only considering the minimal values of J with respect to β_0 and presented in Fig. 4. Clearly a distinct local minimum cannot be found. There is a minimal flat profile (black in Fig. 4) on which the quality of the function fitting is not distinguishable anymore. Furthermore we see that there exists a unique minimum not only in (b, β_0) if $a = 0$ but also in (a, β_0) if $b = 0$. This suggests that either $(u + v)^a = 1$ or $(uv)^b = 1$ holds for this FBSA process. In order to

Table 3
Optimal objective function values and optimal parameters for the reference experiment. The optimization run in the first row does not reach a global minimum due to noise in the measured particle size distribution. The optimizations runs in rows two and three reach two different sets of optimal parameters with nearly the same objective function value. In the last optimization run a set of optimal parameters with a = 0 is found.

Optimization run	J^{opt}	a^{opt}	b^{opt}	$\log_{10}\beta_0^{opt}$
2	2.2387	0.41	−0.529	−21.85
3	0.473	−0.024	0.275	−7.83
3	0.467	0.502	0.553	−19.61
4	0.468	0	0.207	−14.7

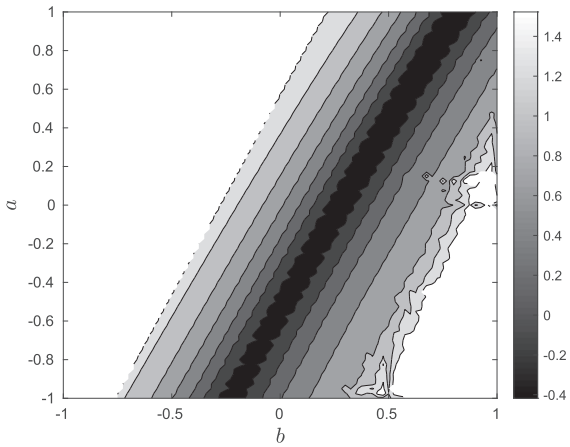

Fig. 4. Sampled objective function values over parameters a and b for the reference experiment. Only the optimal value with respect to β_0 is presented on a logarithmic scale. Shades from black to white correspond to low and high values of J. Parameter combinations where the ode-solver did not converge are white. The black area represents an optimal curve in the parameter space.

reduce the number of kernel parameters we chose (arbitrarily) to set $a = 0$ for the reference experiment.

Samplings for the other experiments show similar results. Therefore the regularized objective function will be used for all further parameter identifications. For the reference experiment the measured steady state (NVD) is presented in Fig. 5 and compared to the simulated NVD using the optimal parameter vector with $a = 0$. The function fit is, except for the primary particle peak, nearly ideal. The resulting coalescence kernel is presented in Fig. 6. For a better presentation the kernel is transformed into diameter coordinates d and d' using Eq. 2. Clearly the values of β decrease with increasing particle diameter which is in agreement with the physical model of particle coalescence presented in [11].

4.1.2. Parameter identifiability and confidence intervals

In this section the structural identifiability of the parameters is investigated. Fig. 4 suggests that the original parameter identification problem with three parameters is overparametrized and therefore structurally not identifiable. In order to overcome this problem the optimization problem was regularized. In this subsection structural parameter identifiability is checked for the regularized problem according to Section 3.

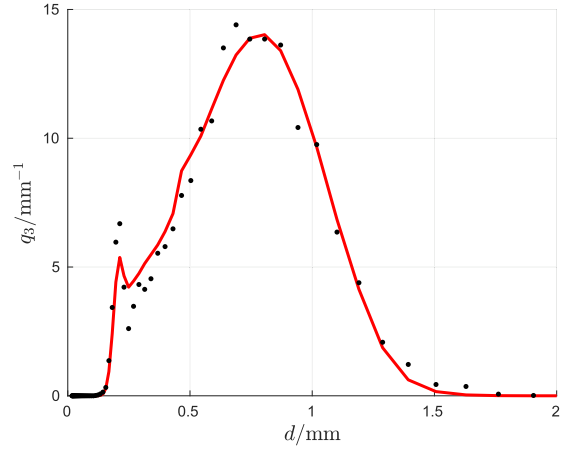

Fig. 5. Measured (black) and simulated (red) NVD at steady state for the reference experiment with Kapur kernel.

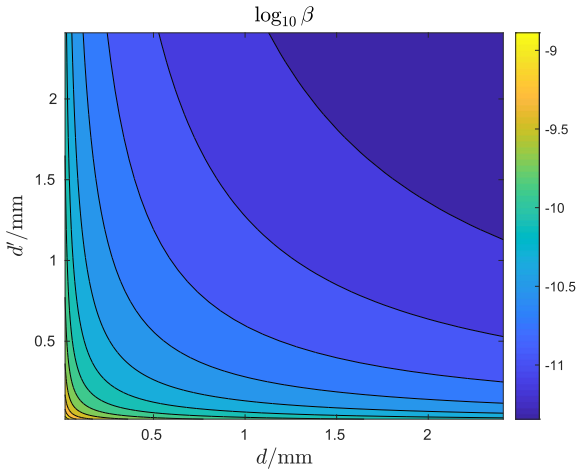

Fig. 6. Logarithmic contour plot of the identified kernel $\beta = \beta_0 \beta(d, d')$ ind diameter coordinates for the reference experiment.

In Fig. 7 the re-estimated optimal objective function J^{opt} is plotted over fixed values for β_0. Since this function has a local minimum, the parameter is structurally identifiable. The same holds for parameter b, presented in Fig. 8. Since a is always equal to 0, investigating the identifiability is omitted.

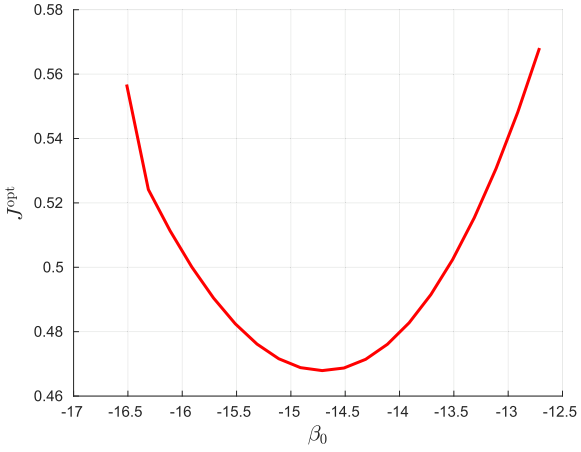

Fig. 7. Optimal objective function for fixed values of β_0.

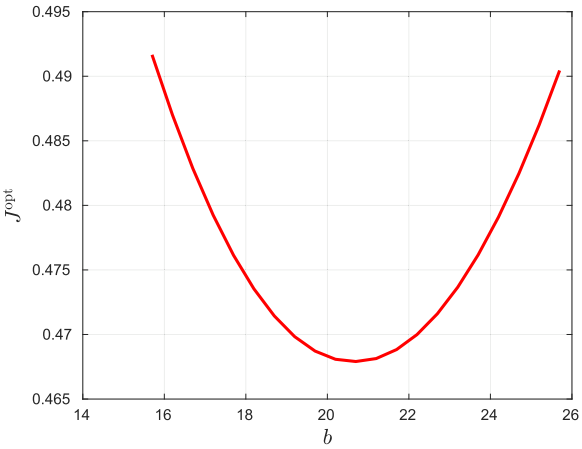

Fig. 8. Optimal objective function for fixed values of b.

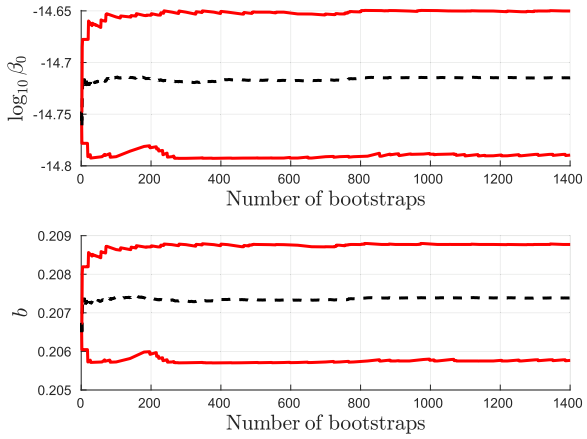

(a) Mean values (black) and 95 %-Confidence intervals (red) for parameter β_0 (top) and b (bottom)

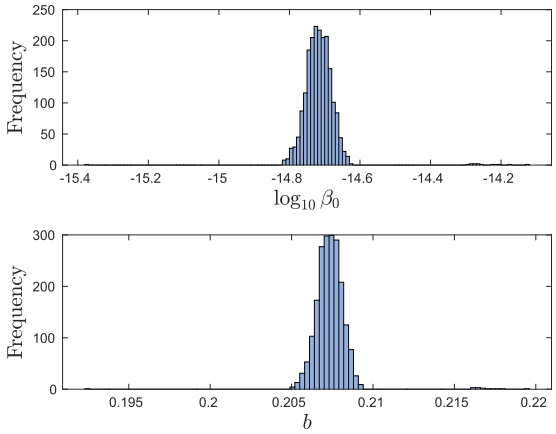

(b) Histograms for estimated parameters β_0 (top) and b (bottom)

Fig. 9. Mean values, confidence intervals and histograms for the parameter estimates.

In order to asses the quality of the parameter identification with respect to uncertainties resulting from measurement, confidence intervals for b and β_0 are presented. Here a 95%-interval is used by setting $\alpha = 0.05$. The mean values and confidence intervals for parameters β_0 and b converge by increasing the number of bootstraps used as presented in Fig. 9a. The corresponding histograms are presented in Fig. 9b.

4.2. Experiments with one parameter variation

In the previous section a process model utilizing a Kapur kernel was fitted to the reference experiment and good results were achieved. In order to identify the influence of the process conditions on the agglomeration kernel, the regularized parameter optimization is conducted for every experiment presented in Table 2 and the results are interpreted. At the end of this subsection the optimal parameters as well as the optimal objective function values are gathered in Table 4.

4.2.1. Influence of gas inlet temperature

In the experiments T1, REF and T2 the gas inlet temperatures is varied from 80 °C to 90 °C and to 100 °C. The particles become smaller with increasing temperature. While experiments T1 and REF are clearly distinguishable, T2 and REF are not, however it is clear that higher temperatures lead to smaller particles. During the process the temperature mainly influences the drying time of the binder solution droplets on the particles. It is assumed that the reduced drying time due to higher temperatures reduces the probability of coalescence between particles [38].

In Fig. 10 the simulated NVDs are compared to the measurements. Clearly the fittings are satisfactory, except for the primary particle peaks. A nearly linear trend can be observed for the identified parameters as presented in Fig. 18.

4.2.2. Influence of primary particle feed rate

The primary particle feed rates are varied from 150 g min^{-1} to 250 g min^{-1} to 350 g min^{-1} in the experiments F1, REF and F2. Interestingly a higher particle feed rate leads to smaller particles. In Strenzke et al. [38] this is explained by a smaller spray-to-surface ratio, i.e. an increased number of primary particles leads to a higher total particle surface. In combination with a constant spray rate the probability of a particle collision at a wet surface spot is decreased. Therefore the particle feed rate has only an indirect effect on the agglomeration kernel. However, under the reasonable assumption that the primary particles are responsible for

Table 4
Optimal objective function values and optimal parameter values for the kapur kernel. As expected the optimal values for parameter a are negligibly small for all experiments and therefore neglected in the table.

Experiment	J^{opt}	b^{opt}	$\log_{10}\left(\beta_0^{\text{opt}}\right)$
REF	0.468	0.207	−14.7
T1	0.644	0.36	−17.5
T2	0.408	0.084	−11.9
F1	1.088	0.74	−24.1
F2	0.626	0.059	−11.9
NA1	0.615	0.29	−15.9
NA2	0.36	0.175	−14.3
S1	0.52	0.230	−15.4
S2	0.503	0.28	−15.8
FA1	0.421	0.200	−14.5
FA2	0.497	0.235	−15.3
BC1	0.531	0.062	−12.1
BC2	0.530	0.275	−15.8
CA1	0.600	0.37	−17.4
CA2	0.471	0.076	−12.39

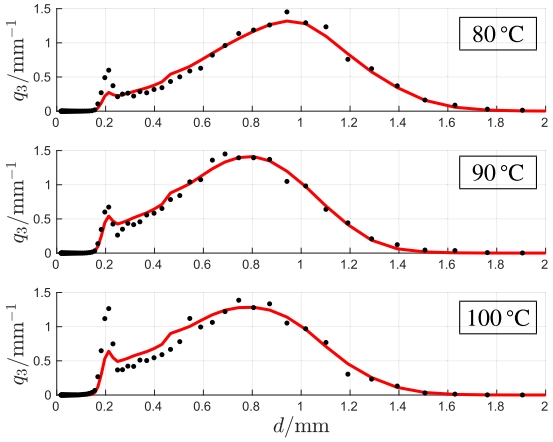

Fig. 10. Measured (black) and simulated (red) particle size distribution steady states for experiment T1, REF and T2 simulated with optimal Kapur parameters obtained from the regularized parameter estimation algorithm.

the majority share of the total particle surface, the influence of $\dot{M}_f$ on the kernel parameters can be investigated directly.

The simulated steady states of the particle size distributions with identified parameters are presented in Fig. 11. The simulations and measurements are in good agreement and a clearly linear trend can be observed for b and β_0 in Fig. 18.

4.2.3. Influence of nozzle air

In this section, the influence of the nozzle air volume flow rate on the Kapur kernel parameters is investigated. The experiments NA1, REF and NA2 where the nozzle air volume flows vary from 40 l min^{-1} to 60 l min^{-1} and to 120 l min^{-1} are considered. The nozzle air flow determines the atomization of binder droplets. Increasing $\dot{V}_{NA}$ leads to smaller spray droplets which again leads to smaller particles. This is explained by the fast drying of small droplets which effectively reduces the number of droplets available for coalescence [38].

The model clearly represents the influence of the nozzle air as presented in Fig. 12. Parameters b and β_0 are presented in Fig. 18.

4.2.4. Influence of binder spray rate

In the experiments S1, REF and S2 the binder mass flows are varied from 40 g min^{-1} to 45 g min^{-1} to 50 g min^{-1}. A lower spray rate shifts the particle size distribution towards smaller particles. This can be explained analogously to the nozzle air experiments with a smaller spray-to-surface ratio.

In Fig. 13 the simulated NVDs are compared to the measurements. The fits are satisfactory, again except for the primary particle peak. Parameters b and β_0 are presented in Fig. 18 for all three experiments.

4.2.5. Influence of fluidization air

In order to investigate the influence of the fluidization air mass flow rate experiments FA1, REF and FA2 are considered. The respective nozzle air volume flows are $260k$ g min^{-1}, $275k$ g min^{-1} and $290k$ g min^{-1}. A difference in the steady state NVDs is difficult to identify, however if the Sauter diameter is considered as in Strenzke et al. [38], significant differences are visible. This is explained by the concentrated occurrence of particle breakage due to higher air flow velocities which leads to smaller particles. Therefore the identified model with agglomeration kernel parameters presented in Fig. 18 implicitly accounts for breakage effects without an explicit breakage term in the PBE. The resulting simulations are in good agreement with the measurements as presented in Fig. 14.

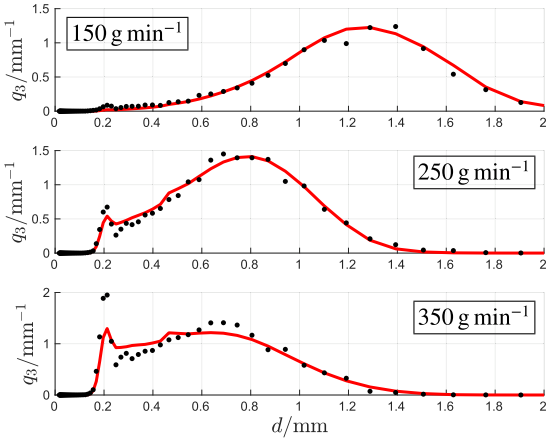

Fig. 11. Measured (black) and simulated (red) particle size distribution steady states for experiment F1, REF and F2 simulated with optimal Kapur parameters obtained from the regularized parameter estimation algorithm.

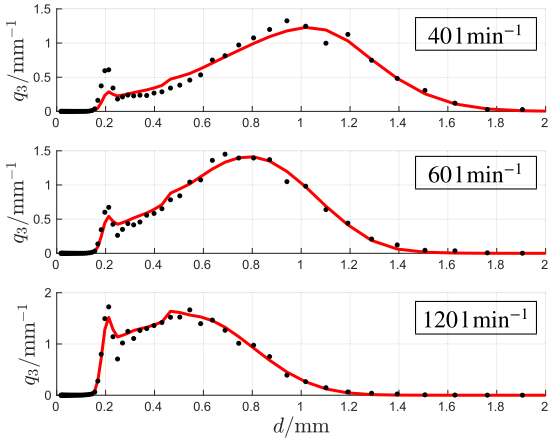

Fig. 12. Measured (black) and simulated (red) particle size distribution steady states for experiment NA1, REF and NA2 simulated with optimal Kapur parameters obtained from the regularized parameter estimation algorithm.

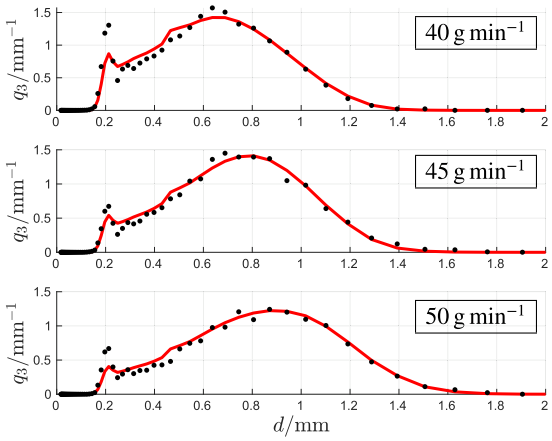

Fig. 13. Measured (black) and simulated (red) particle size distribution steady states for experiment S1, REF and S2 simulated with optimal Kapur parameters obtained from the regularized parameter estimation algorithm.

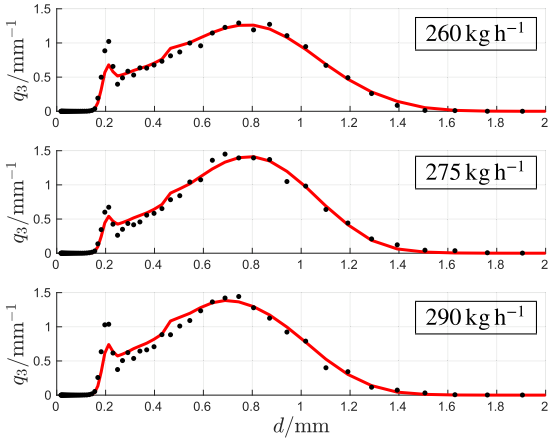

Fig. 14. Measured (black) and simulated (red) particle size distribution steady states for experiment FA1, REF and FA2 simulated with optimal Kapur parameters obtained from the regularized parameter estimation algorithm.

4.2.6. Influence of binder content

For the investigation of the binder content influence, experiments BC1, REF and BC2 are considered. The respective binder mass contents are 2%, 4% and 6%. Since the droplet viscosity is increased by higher binder contents, the probability of complete dissipation of kinetic energy at particle collisions is also increased [11]. Therefore a higher initial binder concentration leads to bigger particles. This dependency is captured by the fitted model, as presented in Fig. 15, the only exception is the primary particle peak in experiment BC1. As in experiment F2 the Kapur kernel is not able to capture the discontinuity between the large primary particle peak and a product particle peak close to it. The identified parameters are presented in Fig. 18. The connection between x_b and the kernel parameters can be modelled approximately by a linear function.

4.2.7. Influence of classification air

The classification air flow affects the quality of separation of bed and product particles [25,15] and therefore the bed PSD by influencing the term $\dot{n}_{out}$ in Eq. 5. However the question is whether $\dot{M}_{CA}$ also affects the agglomeration behavior and thus the agglomeration kernel. By computing the withdrawal term as described in Section 2 the influence on the separation is taken into account. Thus, only effects on the kernel should be detected by the parameter identification algorithm. If there is no (significant) influence on the agglomeration itself, the kernel parameters should be close to those of the reference experiment. However, an explicit influence of $\dot{M}_{CA}$ on T_{sep} can not be deduced from the identified separation functions presented in Fig. 16. Reasons for this non-ideal classification are discussed for example in Müller et al. [24].

Nevertheless the kernel parameters are identified. Fig. 17 shows that the parameter estimation provides a model in good agreement with the measurements. The clearly distinguishable parameters in Fig. 18 indicate a significant influence on the agglomeration behavior, which is explained analogously to the fluidization air experiments by occurrence of particle breakage [38].

4.2.8. Summary

The results from the experiments with only one varied parameter are summarized in Table 4. Overall the model is in good agreement with the all experiments.

The parameter curves presented in Fig. 18 suggest that the dependencies between the process parameters π_i and the model parameters when only one parameter is varied, can be modeled as quadratic functions of the process parameters

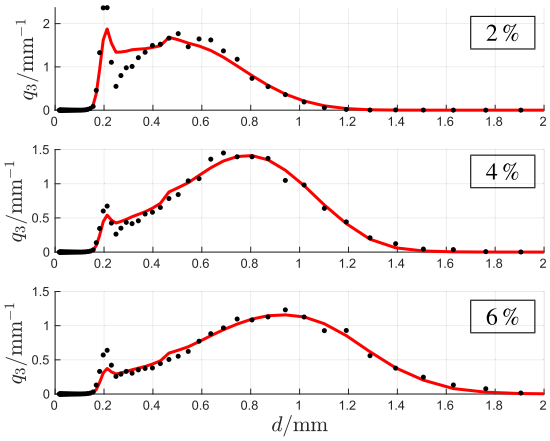

Fig. 15. Measured (black) and simulated (red) particle size distribution steady states for experiment BC1, REF and BC2 simulated with optimal Kapur parameters obtained from the regularized parameter estimation algorithm.

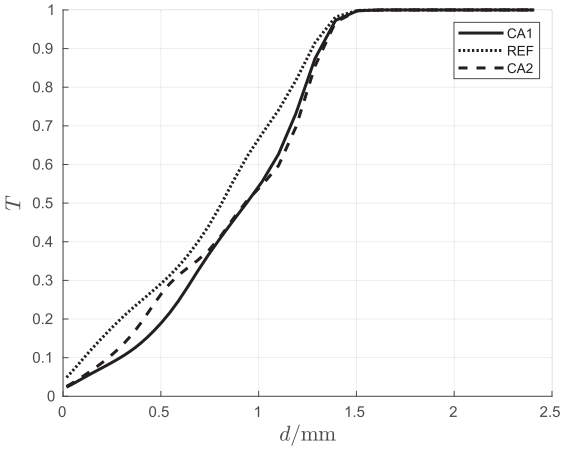

Fig. 16. Steady state classification functions for experiments CA1, REF and CA2. An parametric influence on the classification function is not evident from these functions.

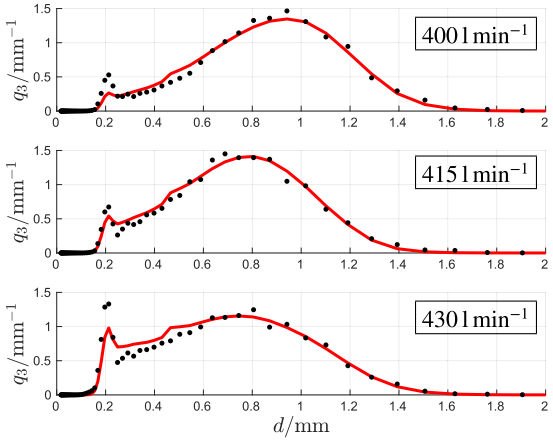

Fig. 17. Measured (black) and simulated (red) particle size distribution steady states for experiment CA1, REF and CA2 simulated with optimal Kapur parameters obtained from the regularized parameter estimation algorithm.

$$\beta_0 = f_\beta(\pi_i) = c_{2,\beta}\pi_i^2 + c_{1,\beta}\pi_i + c_{0,\beta} \tag{21}$$

$$b = f_b(p_i) = c_{2,b}\pi_i^2 + c_{1,b}\pi_i + c_{0,b}, \tag{22}$$

whereas the second order coefficient is nearly equal to 0 for the temperature and feed rate. This provides the opportunity to use the model for predicting particle size distributions when the process parameters are varied within the investigated bounds. For extension to process parameter values outside these bounds, additional experiments need to be performed and incorporated into the estimation procedure.

In order to validate these functions new experiments have to be conducted where the process conditions are set to values inside and possibly outside the respective intervals.

If the optimal parameters b and β_0 are plotted against each other on a logarithmic scale, a clear linear trend can be observed (Fig. 19). A linear regression analysis gives a coefficient of determination $R^2 = 0.994$. While the linear trend is difficult to explain in terms of process understanding, it still presents the possibility to further reduce the number of model parameters to 1 by expressing b in terms of β_0 or vice versa.

4.3. Experiments with multiple parameter variations

One interesting question concerns the validity of functional dependencies (Eq. 21 and 22) when more than one process condi-

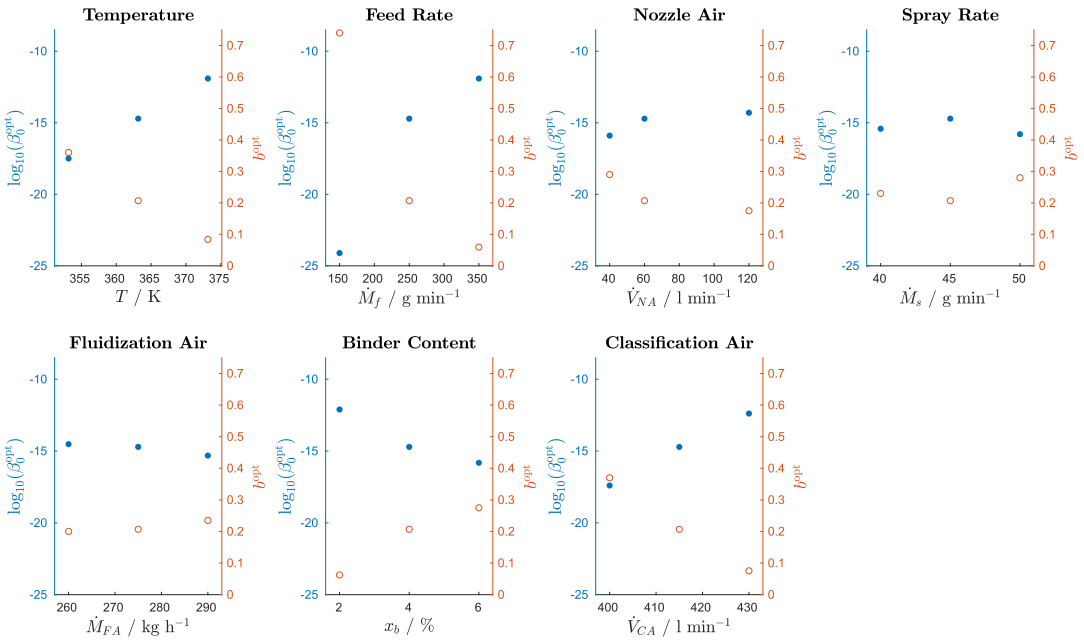

Fig. 18. Identified parameters b and $\log_{10}(\beta_0)$ for the seven sets of experiments.

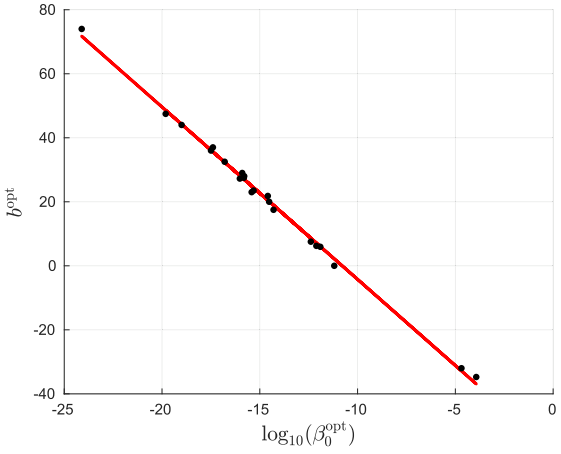

Fig. 19. Identified parameters b^{opt} over the logarithm of β_0^{opt} together with the linear regression curve.

tion is changed. It is natural to assume that additionally to the polynomial behavior on the principal axes, coupled effects occur. In order to investigate this case, additional experiments were conducted. Due to the high number of possible experiments when combinations of 7 parameters are varied, the number of regressors was reduced to 3, namely the feed rate, gas inlet temperature and spray rate. They were chosen because they have a significant effect on the particle size distribution and are easy to adjust at the plant and therefore are excellent candidates for manipulation in process control applications. The parameters for the 8 experiments are presented in Table 5, however two of them had to be terminated early and can not be used in this study. As in the previous section parameters b and β_0 are identified by optimization.

Based on the one-dimensional case a multi-dimensional polynomial of degree two is chosen as ansatz for f_β and f_b. The coefficients a_i of the resulting polynomial function

$$\beta_0 = a_1\pi_1^2 + a_2\pi_1 + a_3\pi_2^2 + a_4\pi_2 + a_5\pi_3^2 + a_6\pi_3 + a_7\pi_1\pi_2 + a_8\pi_2\pi_3 + a_9\pi_3\pi_1 + a_{10} \tag{23}$$

of the parameter vector

$$\Pi = \begin{pmatrix}\pi_1\\ \pi_2\\ \pi_3\end{pmatrix} := \begin{pmatrix}\dot{M}_{\text{feed}}\\ \dot{M}_{\text{spray}}\\ T_{\text{g,in}}\end{pmatrix} \tag{24}$$

can be fitted by linear regression. The function for parameter b is defined analogously.

The 10 coefficients in **a** were identified by using the 7 relevant experiments from Table 2 and 6 experiments from Table 5 for b and β_0 respectively. The regression provides good results presented in Fig. 20. Furthermore, the regression shows that parameters a_3 and a_7 are negligibly small for both b and β_0, which means that the terms $T_{\text{g,in}}^2$ and $\left(\dot{M}_{\text{feed}}T_{\text{g,in}}\right)$ in Eq. 23 are not relevant for the computation of β_0 and b. The former realization is in agreement with the findings from the one-parameter-variation case. The latter confirms the explanation of how the particle size is affected by temperature and feed rate in Section 4.2. Since the temperature does not change the total particle surface and the feed rate does not influence the droplet drying there are no coupled effects and both process conditions independently affect the evolution of the particle size.

4.3.1. Parameter identification for the system dynamics

In the previous subsections, only the steady state of the process was considered in the objective function. Hence, the identified model only captures the system behavior near the steady state. The focus of this subsection is on the dynamic behavior, which is investigated for the reference experiment as an example.

In Fig. 21 the measured $q_{3,\text{meas}}(t,x)$ is compared with the simulated $q_{3,\text{sim}}(t,x)$ at selected time instants. In order to compute $q_{3,\text{meas}}(t,x)$ the identified steady state parameters from Section 4.1 were used.

In the transition time between $t = 0min$ and $t = 20min$ the process model does not capture the process behavior. Between $t = 20min$ and $t = 80min$ the fit is good, while it is nearly optimal when the system reaches the steady state around $t = 80min$.

In order to find model parameters a, b and β_0 that are able to capture the non-steady state behavior of the process, the optimiza-

Table 5
Overview of experiments with multiple parameters varied simultaneously.

Experiments	Process Conditions			Comments
	$\dot{M}_{\text{feed}}$ g/min	$T_{\text{g,in}}$ °C	$\dot{M}_{\text{spray}}$ g/min	
F1T1S1	150	80	40	
F1T1S2	150	80	50	terminated early
F1T2S1	150	100	40	interrupted
F1T2S2	350	100	50	
F2T1S1	350	80	40	
F2T1S2	350	80	50	
F2T2S1	350	100	40	
F2T2S2	150	100	50	

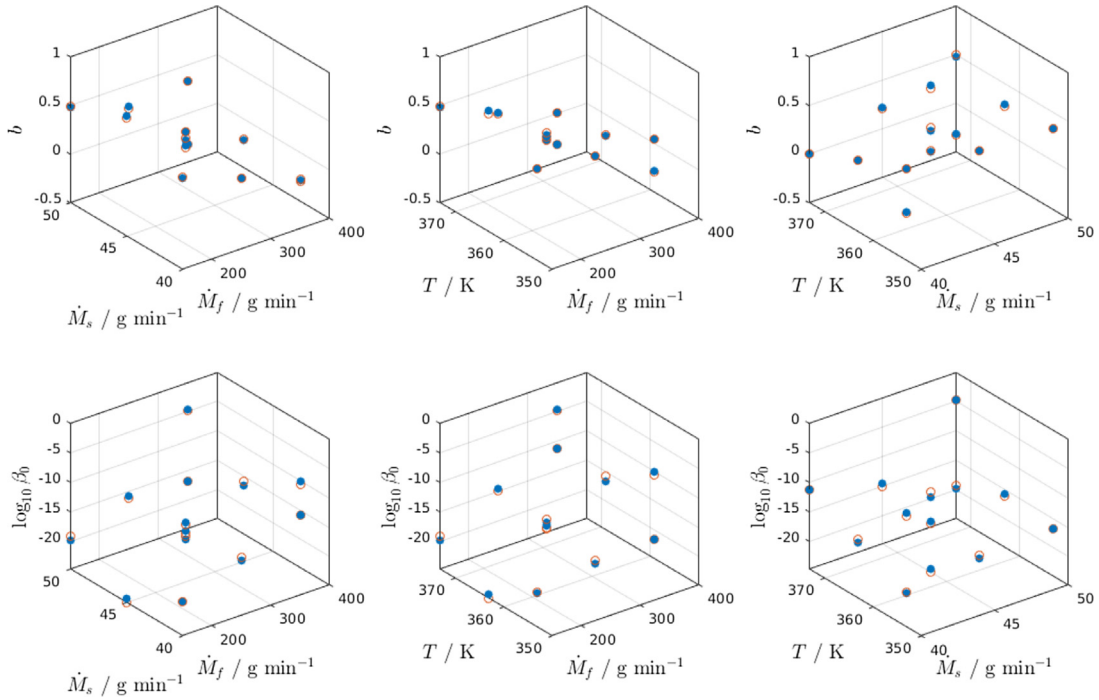

Fig. 20. Graphical presentation of the 3-dimensional linear regression for parameter b (top) and β_0 (bottom), measurements are blue, predicted values red. The coefficients of determination are $R^2 = 0.985$ for b and $R^2 = 0.965$ for β_0.

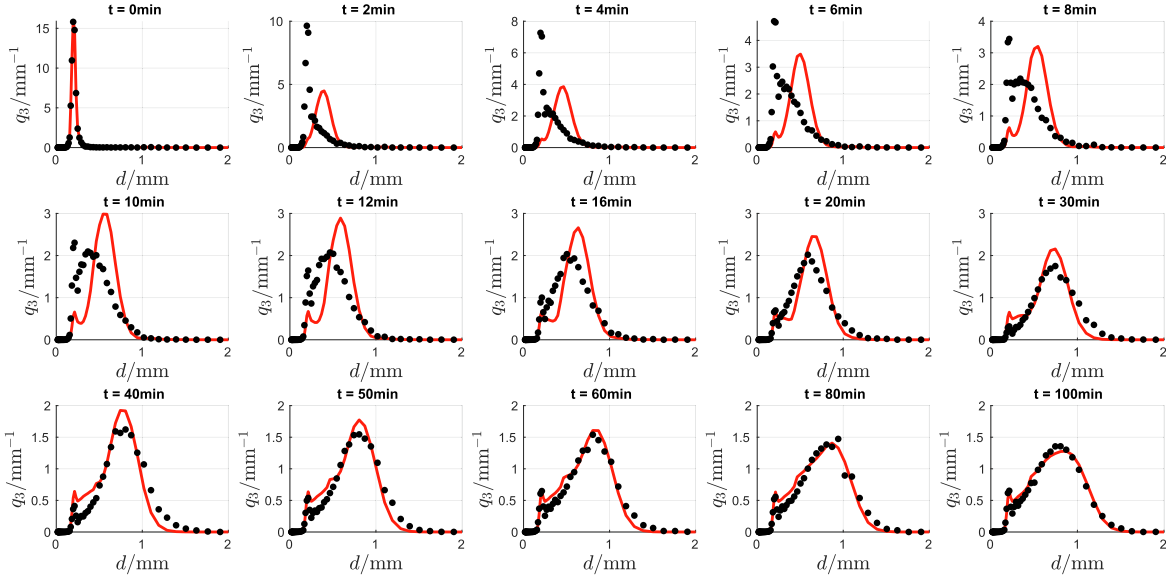

Fig. 21. Comparison between measured (black) and simulated $q_3(t,x)$ (red) for selected time steps within the whole experimental time domain.

tion has been repeated considering the whole time domain in the objective function. However, the optimal parameters do only change negligibly compared to steady state identification and the process model is still not able to capture the process dynamics at the beginning of the measurements. Therefore, we conclude that the process model with constant kernel parameters is not able to capture the start-up dynamics appropriately. In accordance with the results in Golovin et al. [14] there seems to be a fundamental difficulty in predicting the first minutes of the process with a set of constant parameters, however from a practical point of view the first minutes of the process can be neglected if the process is in stationary state for a much larger time.

5. Conclusion

This contribution dealt with the modeling of fluidized bed spray agglomeration based on a population balance equation approach. In particular, the parameters of the agglomeration kernel function were identified. Therefore the PBE was fitted to a set of experiments with varying process parameters by minimizing the least square error. Process conditions like fluidization properties and drying conditions were varied systematically by varying adjustable parameters. These include the gas inlet temperature, fluidization and classification air flows, binder concentration and atomization as well as spray rate and the primary particle feed rate.

From a set of both, physically based and empirical kernel functions, the three-parametric Kapur kernel was identified as the best choice to represent the agglomeration behaviour in the model. In the course of the identification procedure, the number of kernel parameters could be reduced to only one which is a useful result regarding future parameter identifications on the one hand and general model reduction considerations on the other hand. The first main result of this contribution is the qualitatively and quantitatively good agreement between the process model and the experimental data for every experiment considered. Furthermore, two basic requirements for the identified model parameters are shown to be true. They are precise within a small confidence interval with respect to a certain class of measurement noise and structurally identifiable.

The second main result of this contribution is that the influence of the seven process parameters on the steady state particle size distribution can be mapped quantitatively onto the kernel parameters, i.e. the adjustable process conditions appear in the PBE. This is always possible if one process parameter is varied at a time but also for multiple parameter variations if only the spray and feed rate as well as the gas inlet temperature are varied simultaneously. The explanations for the influence of the temperature and the feed rate on the agglomerate size presented in Strenzke et al. [38] are in accordance with the parameter mappings in this contribution.

In summary, the population balance equation together with the identified parameters and the connection to the process conditions represent a sound base for subsequent applications in process optimization and model-based control which is one possible future research direction.

Additionally, the presented model can be extended in three possible directions: At first, the influence of further process conditions can be examined, especially the interactions between different process parameters have not been conclusively clarified. To this end, further experimental efforts are required. Moreover, the transient process dynamics are not reflected by the process model quantitatively. The current model can be extended in this direction for example by introducing time-variant model parameters. Finally, further important distributed particle properties such as porosity could be incorporated as additional independent variables into a multivariate PBE.

Declaration of Competing Interest

The authors declare that they have no known competing financial interests or personal relationships that could have appeared to influence the work reported in this paper.

Acknowledgements

This work is funded by the European Regional Development Fund (ERDF) project “Center of Dynamic Systems”. The financial support is hereby gratefully acknowledged.

References

[1] A. Adetayo, J. Litster, S. Pratsinis, B. Ennis, Population balance modelling of drum granulation of materials with wide size distribution, Powder Technol. 82 (1995) 37–49.
[2] A. Barkouti, C. Turchiuli, J.A. Carcel, E. Dumoulin, Milk powder agglomerate growth and properties in fluidized bed agglomeration, Dairy Sci. Technol. 93 (2013) 523–535.
[3] A. Bück, R. Dürr, M. Schmidt, E. Tsotsas, Model predictive control of continuous layering granulation in fluidised beds with internal product classification, J. Process Control 45 (2016) 65–75.
[4] A. Bück, E. Tsotsas, Agglomeration, in: B. Caballero, P.M. Finglas, F. Toldrá (Eds.), Encyclopedia of Food and Health, Academic Press, Oxford, 2016, pp. 73–81.
[5] P. Bühlmann, S. van de Geer, Statistics for High-Dimensional Data, Springer, Berlin, Heidelberg, 2011.
[6] M. Dadkhah, E. Tsotsas, Influence of process variables on internal particle structure in spray fluidized bed agglomeration, Powder Technol. 258 (2014) 165–173.
[7] J. Du, A. Bück, E. Tsotsas, Influence of process variables on spray agglomeration process in a continuously operated horizontal fluidized bed, Powder Technol. 363 (2020) 195–206.
[8] R. Dürr, Parameter estimation, in: A. Martynenko, A. Bück, (Eds.), Intelligent Control in Drying, Advances in Drying Science and Technology. chapter 3, CRC Press, 2019, pp. 27–51.
[9] R. Dürr, S. Palis, A. Kienle, Online parameter identification of facet growth kinetics in crystal morphology population balance models, Proc. Eng. 102 (2015)1336–1345. New Paradigm of Particle Science and Technology Proceedings of The 7th World Congress on Particle Technology.
[10] H. Eisenschmidt, M. Soumaya, N. Bajcinca, S. Le Borne, K. Sundmacher, Estimation of aggregation kernels based on laurent polynomial approximation, Comput. Chem. Eng. 103 (2017) 210–217.
[11] B.J. Ennis, G. Tardos, R. Pfeffer, A microlevel-based characterization of granulation phenomena, Powder Technol. 65 (1991) 257–272.
[12] A.M. Golovin, The Solution of the Coagulation Equation for Raindrops. Taking Condensation into Account, Soviet Physics Doklady 8 (1963) 191.
[13] I. Golovin, E. Otto, R. Dürr, S. Palis, A. Kienle, Lyapunov-based online parameter estimation in continuous fluidized bed spray agglomeration processes, IFAC-PapersOnLine 52 (2019) 329–334.
[14] I. Golovin, G. Strenzke, R. Dürr, S. Palis, A. Bück, E. Tsotsas, A. Kienle, Parameter identification for continuous fluidized bed spray agglomeration, Processes 6 (2018) 246.
[15] S. Heinrich, M. Peglow, M. Ihlow, M. Henneberg, L. Mörl, Analysis of the start-up process in continuous fluidized bed spray granulation by population balance modelling, Chem. Eng. Sci. 57 (2002) 4369–4390.
[16] H. Hulburt, S. Katz, Some problems in particle technology: A statistical mechanical formulation, Chem. Eng. Sci. 19 (1964) 555–574.
[17] M. Hussain, J. Kumar, M. Peglow, E. Tsotsas, Modeling spray fluidized bed aggregation kinetics on the basis of monte-carlo simulation results, Chem. Eng. Sci. 101 (2013) 35–45.
[18] M. Hussain, J. Kumar, E. Tsotsas, Modeling aggregation kinetics of fluidized bed spray agglomeration for porous particles, Powder Technol. 270 (2015) 584–591.
[19] M. Joshi, A. Seidel-Morgenstern, A. Kremling, Exploiting the bootstrap method for quantifying parameter confidence intervals in dynamical systems, Metab. Eng. 8 (2006) 447–455.
[20] P. Kapur, Kinetics of granulation by non-random coalescence mechanism, Chem. Eng. Sci. 27 (1972) 1863–1869.
[21] P.C. Kapur, D.W. Fuerstenau, Coalescence model for granulation, Ind. Eng. Chem. Process Des. Develop. 8 (1969) 56–62.
[22] S.J. Kim, K. Koh, S. Boyd, D. Gorinevsky, ℓ_1 trend filtering, SIAM Rev. 51 (2009) 339–360.
[23] J. Kumar, M. Peglow, G. Warnecke, S. Heinrich, The cell average technique for solving multi-dimensional aggregation population balance equations, Comput. Chem. Eng. 32 (2008) 1810–1830.
[24] D. Müller, A. Bück, E. Tsotsas, Influence of separation properties and processing strategies on product characteristics in continuous fluidized bed spray granulation, Powder Technol. 342 (2019) 572–584.
[25] O. Molerus, H. Hoffmann, Darstellung von Windsichtertrennkurven durch ein stochastisches Modell, Chem. Ing. Tech. 41 (1969) 340–344.

[26] E. Murtoniemi, J. Yliruusi, P. Kinnunen, P. Merkku, K. Leiviskä, The advantages by the use of neural networks in modelling the fluidized bed granulation process, Int. J. Pharm. 108 (1994) 155–164.
[27] C. Neugebauer, E. Diez, A. Bück, S. Palis, S. Heinrich, A. Kienle, On the dynamics and control of continuous fluidized bed layering granulation with screen-mill-cycle, Powder Technol. 354 (2019) 765–778.
[28] E. Otto, C. Neugebauer, S. Palis, A. Kienle, Lyapunov-based online parameter estimation for continuous fluidized bed layering granulation, in: Proceedings of the 21th IFAAC World Congress, 2020.
[29] E. Otto, S. Palis, A. Kienle, Control of continuous fluidized bed spray agglomeration processes [accepted manuscript], 2020b.
[30] S. Palzer, Chapter 13 agglomeration of dehydrated consumer foods, in: A. Salman, M. Hounslow, J. Seville (Eds.), Granulation, volume 11 of Handbook of Powder Technology, Elsevier Science B.V., 2007, pp. 591 – 671.
[31] S. Palzer, Agglomeration of pharmaceutical, detergent, chemical and food powders – similarities and differences of materials and processes, Powder Technol. 206 (2011) 2–17.
[32] M. Peglow, J. Kumar, R. Hampel, E. Tsotsas, S. Heinrich, Towards a complete population balance model for fluidized-bed spray agglomeration, Drying Technol. 25 (2007) 1321–1329.
[33] D. Ramkrishna, Population Balances: Theory and Applications to Particulate Systems in Engineering, Academic Press, 2000.
[34] A. Raue, C. Kreutz, T. Maiwald, J. Bachmann, M. Schilling, U. Klingmüller, J. Timmer, Structural and practical identifiability analysis of partially observed dynamical models by exploiting the profile likelihood, Bioinformatics 25 (2009) 1923–1929.
[35] K.V. Sastry, Similarity size distribution of agglomerates during their growth by coalescence in granulation or green pelletization, Int. J. Miner. Process. 2 (1975) 187–203.
[36] T.E.W. Schumann, Theoretical aspects of the size distribution of fog particles, Quart. J. Roy. Meteorol. Soc. 66 (1940) 195–208.
[37] M.v. Smoluchowski, Drei Vortrage uber Diffusion, Brownsche Bewegung und Koagulation von Kolloidteilchen, Z. Angew. Phys. 17 (1916) 557–585.
[38] G. Strenzke, R. Dürr, A. Bück, E. Tsotsas, Influence of operating parameters on process behavior and product quality in continuous spray fluidized bed agglomeration, Powder Technol. (2020).
[39] H. Tan, A. Salman, M. Hounslow, Kinetics of fluidized bed melt granulation–ii: Modelling the net rate of growth, Chem. Eng. Sci. 61 (2006) 3930–3941.
[40] K. Terrazas-Velarde, M. Peglow, E. Tsotsas, Investigation of the kinetics of fluidized bed spray agglomeration based on stochastic methods, AIChE J. 57 (2011) 3012–3026.
[41] C. Turchiuli, Z. Eloualia, N. El Mansouri, E. Dumoulin, Fluidised bed agglomeration: Agglomerates shape and end-use properties, Powder Technol. 157 (2005) 168–175. 4th French Meeting on Powder Science and Technology.
[42] M. Williams, S. Loyalka, Aerosol science: theory and practice, 1991.